JOURNAL OF GEOPHYSICAL RESEARCH, VOL. 103, NO. A3, PAGES 3969–3981, MARCH 1, 1998

Equatorial density irregularity structures at intermediate scales and their temporal evolution

Hyosub Kil and R. A. Heelis

William B. Hanson Center for Space Sciences, Physics Program, University of Texas at Dallas, Richardson

Abstract. We examine high resolution measurements of ion density in the equatorial ionosphere from the AE-E satellite during the years 1977-1981. Structure over spatial scales from 18 km to 200 m is characterized by the spectrum of irregularities at larger and smaller scales and at altitudes above 350 km and below 300 km. In the low-altitude region, only small amplitude large-scale (λ>5 km) density modulations are often observed, and thus the power spectrum of these density structures exhibits a steep spectral slope at kilometer scales. In the high-altitude region, sinusoidal density fluctuations, characterized by enhanced power near 1-km scale, are frequently observed during 2000-0200 LT. However, such fluctuations are confined to regions at the edges of larger bubble structures where the average background density is high. Small amplitude irregularity structures, observed at early local time hours, grow rapidly to high-intensity structures in about 90 min. Fully developed structures, which are observed at late local time hours, decay very slowly producing only small differences in spectral characteristics even 4 hours later. The local time evolution of irregularity structure is investigated by using average statistics for low- (1%<σ<5%) and high-intensity (σ>10%) structures. At lower altitudes, little change in the spectral slope is seen as a function of local time, while at higher altitudes the growth and maintenance of structures near 1 km scales dramatically affects the spectral slope.

1. Introduction

The equatorial ionosphere contains a vast range of plasma density irregularities with spatial scales varying from several hundred kilometers to a few meters. The generally accepted process for the generation of irregularities is first creation of large-scale density modulations on the bottomside *F* region perhaps by gravity waves, followed by enhancement of density fluctuations by the gravity and electric field induced collisional Rayleigh-Taylor instability. In this process the low-density plasma (bubble) nonlinearly rises to the high-altitude region producing plasma density irregularities also in the topside. The bubble wall becomes steep as it rises, and the operation of drift waves and neutral winds further fragment the large-scale irregularities to smaller and smaller-scale sizes.

The spatial range of irregularities is more than 7 orders of magnitude, so the study of irregularity structure has been performed separately by dividing the scales into several ranges. Among them, intermediate scales (0.1-10 km) [*Kelley et al.*, 1982] are of special interest since the most severe radio scintillation is caused by irregularities in this scale range. In this scale range, numerous measurements by satellite and rocket experiments are also available as well as scintillation observations.

Ionospheric irregularity structures in the intermediate scale may be characterized by the power spectrum of the density fluctuations. The power law is represented by the form $I \propto k^{-n}$, where I is the power spectral density, n is the spectral index, and k is the spatial wave number. The observed spectral indices typically lie in the range -2 to -2.5 [*Dyson et al.*, 1974; *Rino et al.*, 1981; *Livingston et al.*, 1981; *Kelley and McClure*, 1981; *Kelley et al.*, 1982; *Singh and Szuszczewicz*, 1984; *LaBelle and Kelley*, 1986] and are in good agreement with the theoretical prediction and numerical simulation results [*Scannapieco and Ossakow*, 1976; *Chaturvedi and Ossakow*, 1977; *Keskinen et al.*, 1980a, b; *Sudan and Keskinen*, 1984]. But often the observed spectra show a more shallow slope at wavelengths longer than 1 km and a steeper slope at meter scales [*Rino et al.*, 1981; *Kelley et al.*, 1982; *Basu et al.*, 1983; *Valladares et al.*, 1983; *Cragin et al.*, 1985; *Basu and Basu*, 1985]. This break in the spectrum, or the enhancement of power near 1 km, has been explained by energy injection into this scale from turbulence developed on the steep walls of convecting bubbles [*Zalesak et al.*, 1982; *LaBelle and Kelley*, 1986; *Kelley*, 1989] or from the formation of image structures at this scale in the *E* region [*Francis and Perkins*, 1975; *Vickrey et al.*, 1984; *Heelis et al.*, 1985; *LaBelle*, 1985; *LaBelle and Kelley*, 1986; *Heelis and Vickrey*, 1990].

A variability in the spectral index is expected from the results of numerical simulations and theoretical studies. *Zargham and Seyler* [1987] and *Kelley et al.* [1987] showed an anisotropy in the irregularity density structure from model calculations, displaying a nearly sinusoidal fluctuation in the horizontal direction and a shocklike structure in the vertical direction. This would imply significant variations of the power spectrum due to changes in the angle between the satellite or rocket motion and the irregularity structure. The nonlinear theory applied to spread *F* by *Sudan and Keskinen* [1984] also predicts a possible change of the spectral form depending on the turbulence strength, which again depends on the wave number.

With ever increasing use of artificial satellites for communication, the electron density irregularities in the ionosphere have attracted more attention since they cause phase and amplitude scintillations in satellite communication signals at VHF, UHF, and even microwave frequencies. The

Paper number 97JA03344.
0148-0227/98/97JA-03344$09.00

magnitude of scintillation decreases as the radio frequency increases, but even as high as 6 GHz [*Basu and Larson*, 1995] scintillation may possibly cause problems.

Strong scintillation occurs when the Fresnel dimension of a propagating radio wave is of the order of the irregularity scale in the ionosphere [*Briggs and Parkin*, 1963]. The Fresnel dimension is approximately 1 km at VHF but decreases as the frequency increases. For a long time the interpretation of scintillation measurements has been based on the assumption of a Gaussian spectral shape. Later, a power law was broadly adopted in the analysis of in situ and ground scintillation measurements. *Basu et al.* [1976] applied a phase screen model developed by *Rufenach* [1975] to convert the direct measurements of density irregularity by the OGO 6 satellite to the S_4 index. They assumed the spectral shape was either Gaussian or a three-dimensional power law with spectral index n=-4 and showed that the S_4 value is sensitive to the assumed spectral shape at high frequencies. Among the parameters in the equation, the perturbation magnitude ΔN was provided from the observations but the outer scale and the spectral index for the irregularity spectrum has to be assumed. Thus the spectral shape of observed irregularities is an important contribution to scintillation models.

In addition to providing correct input parameters to scintillation models, the power spectrum itself reveals useful information about irregularity structure. Spectral analysis is a very useful method for handling huge amounts of data since most of the important information is reduced to only a few spectral parameters. From the spectral shape we can identify which scale is dominant for a given irregularity structure, and from the variation of spectral parameters with local time we can estimate how the irregularity structure evolves in time. For this study, first we investigate individual density structures and the associated power spectrum to establish the relationships that exist. Then we investigate the variations of average spectral parameters with local time.

In section 2 we briefly mention the satellite measurements and describe the spectral analysis process. In section 3 we present the results from individual cases and statistical studies. In section 4 we discuss the results and conclude in section 5.

2. Instrumentation and Data Analysis

We analyze ion density measurements made by the retarding potential analyzer (RPA) on the AE-E satellite. A detailed description of the instrumentation and the principles of operation are given by *Hanson et al.* [1973] and *Hanson and Heelis* [1975]. The satellite sampled the equatorial ionosphere (approximately -40° to 40° in magnetic latitudes) in a 19° inclination orbit during the years 1977-1981 with altitude ranging from about 240 to 470 km. For 3 s out of every 8 s the RPA provided continuous measurements of the total ion concentration in a "duct" mode. It had two modes giving either 70-m or 35-m spatial resolution. We selected 256 points from either of the two modes to always provide a spatial resolution of 70 m. In this analysis the time span for one RPA duct segment is 2.3 s with 8.93-ms intervals (Δt) between each point. The Nyquest frequency (f_N) is calculated from the relation $f_N = 1/(2\Delta t)$, which gives 56 Hz. The frequency (f) can be converted to the wavelength (λ) using the relation $\lambda = v/f$, where v is the satellite velocity. If v is assumed to be 8 km s^{-1} and structures are assumed to be stationary, we can identify a minimum irregularity scale of 142 m. Each duct segment was subject to a power spectral analysis using a fast Fourier transform (FFT). For this purpose we linearly detrended the ion concentration data and obtained $\Delta N/N_o$, where ΔN is the difference from the average density (N_o) obtained from the trend line. A Hanning window is applied to the time series of $\Delta N/N_o$ prior to a FFT to obtain the power spectrum of $\Delta N/N_o$. The spectrum is fit in two frequency intervals to obtain

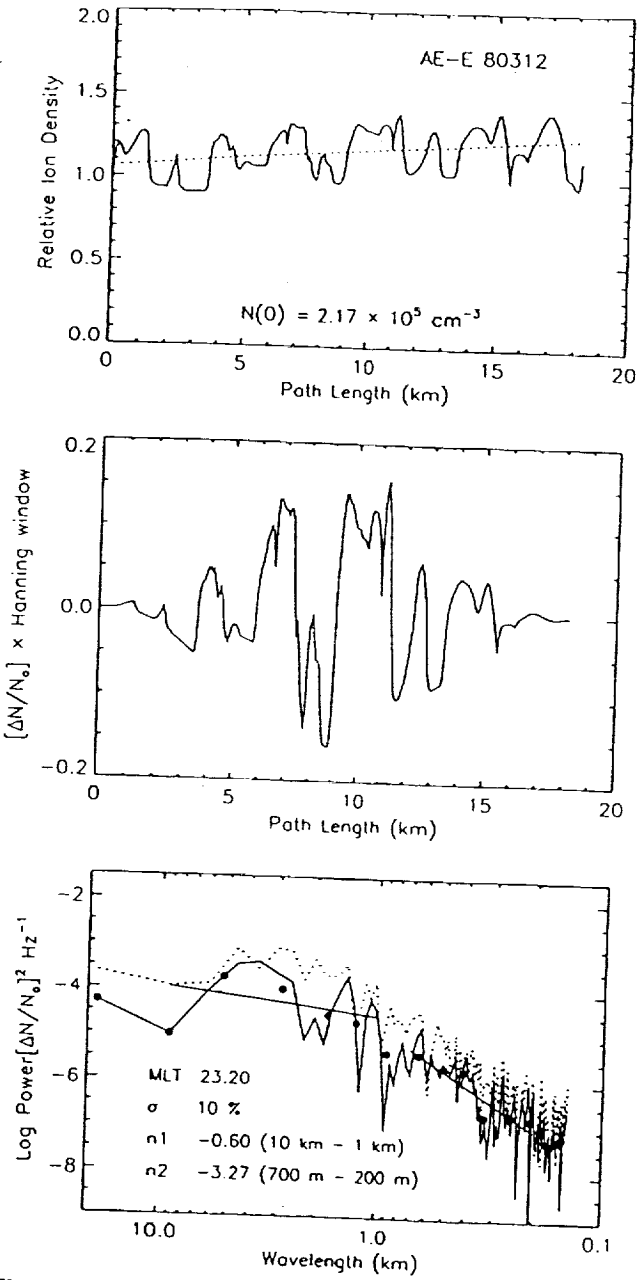

Figure 1. Measurement of ion density by "duct" mode and its power spectrum. (top) Relative ion density (solid line) and trend line (dotted line). $\Delta N/N_o$ is calculated from this trend line, and (middle) $\Delta N/N_o$ after applying Hanning window. (bottom) Resulting power spectrum with (solid curve) and without (dotted curve) applying Hanning window. From the two linear square fitting lines spectral indices at kilometer (n1) and meter (n2) scales are obtained. The solid circles are average spectral densities at each wavelength.

separate spectral indices in large-wavelength (10-1 km) and small-wavelength(700-200 m) ranges. Our data set includes general information such as date, universal time, local time, longitude, magnetic and geographic latitude, and physical quantities like average density, standard deviation in $\Delta N/N_o$, spectral indices, and Kp value. The information in the power spectrum was retained by storing average powers at 15 frequencies.

The top panel of Figure 1 shows a typical 2.3-s segment of the recorded ion concentration from the RPA duct mode. The dotted line shows the detrended straight line used to derive the perturbation densities and the rms deviations in the signal during the 2.3-s period. This deviation is noted as σ in the lowest panel. The middle panel shows the relative density variations after a Hanning window is applied to the data to ensure that the end points match, and a discrete FFT procedure may be applied to the data. The bottom panel shows the resulting power spectrum obtained from the FFT procedure. In this panel is shown the results with (solid line) and without (dotted line) the Hanning window applied. It should be noted that the power spectrum shows reduced powers in frequency space after the Hanning window is applied. Also shown in this lower panel are the results of straight-line fitting in the two-wavelength regimes to obtain spectral slopes (or spectral indices) in the spatial regions near 5 km (n1) and 500 m (n2). The average powers at 15 frequencies are shown by solid circles.

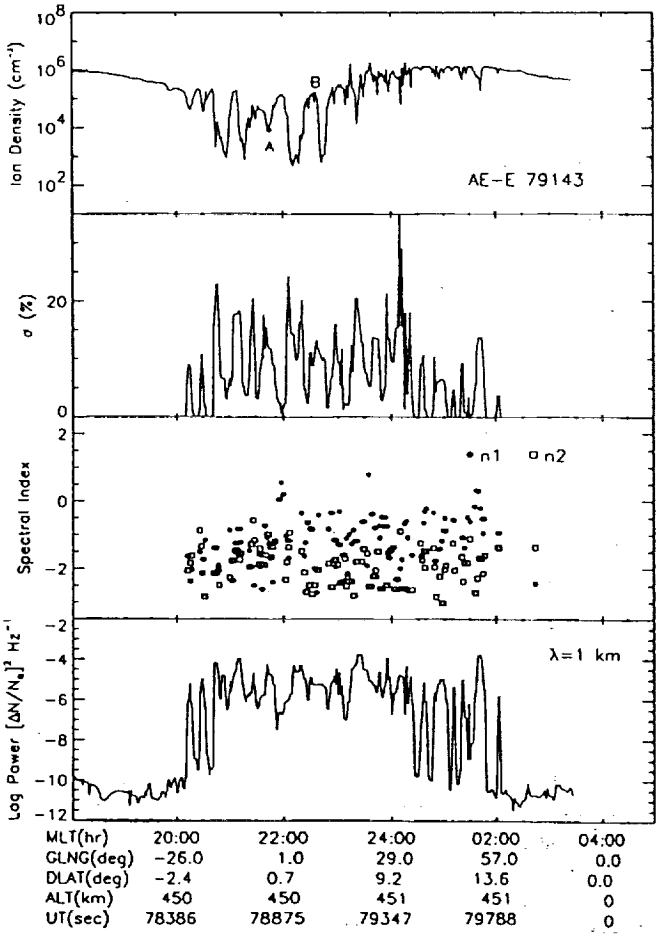

Figure 2. Ion density measurements with σ, spectral index, and power during nighttime at 450 km altitude. MLT, magnetic local time; GLNG, geophysical longitude; DLAT, dip latitude; ALT, altitude; UT, universal time.

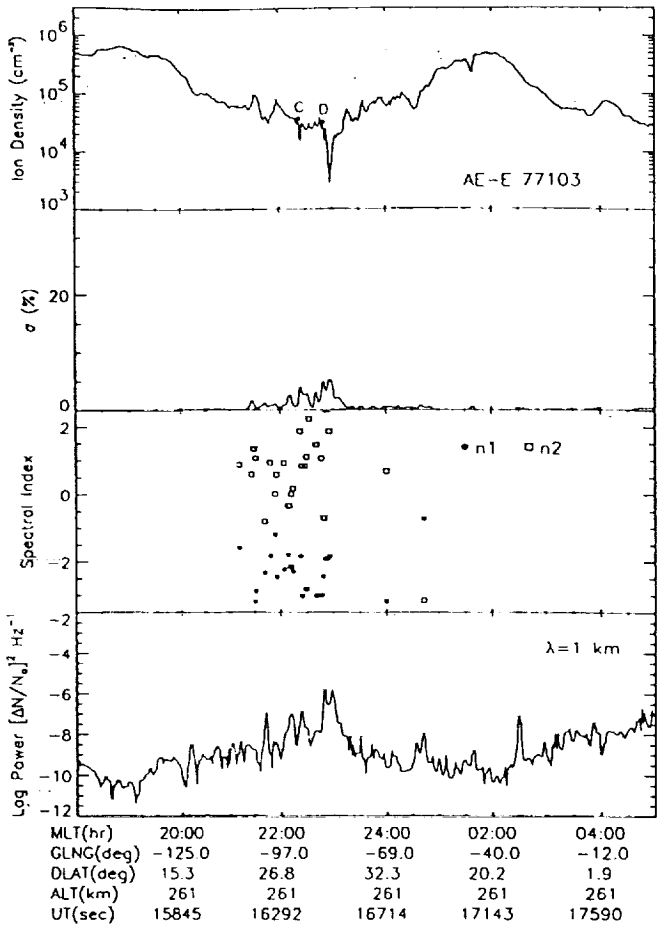

Figure 3. Ion density measurements with σ, spectral index, and power during nighttime at 260 km altitude.

3. Observations

Large-scale density irregularity regions show different features at the high- and low-altitude extents encountered by AE-E [*Kil and Heelis*, 1998], but the small-scale density structure inside the large structure is also largely different in the two-altitude regions. The top panel in Figure 2 shows the density structure observed near 450 km altitude with bottom panels showing the rms deviations s, the spectral indices, and the power spectral density at 1 km, respectively. The density-depleted regions are well correlated with large values of σ and power. There is little difference in the spectral indices at the kilometer and meter scales in the early local times, but the spectral index at kilometer scales increases while that at meter scales decreases at later times. The structured region occupies about 6 hours in local time and therefore the local time variations of spectral characteristics may reflect some part of the observed signature. But it should be noted that bubbles observed at later times may not always be those that have evolved from earlier times.

Figure 3 shows the ion density, σ, spectral indices, and power at 1 km measured near 260 km in the same format as

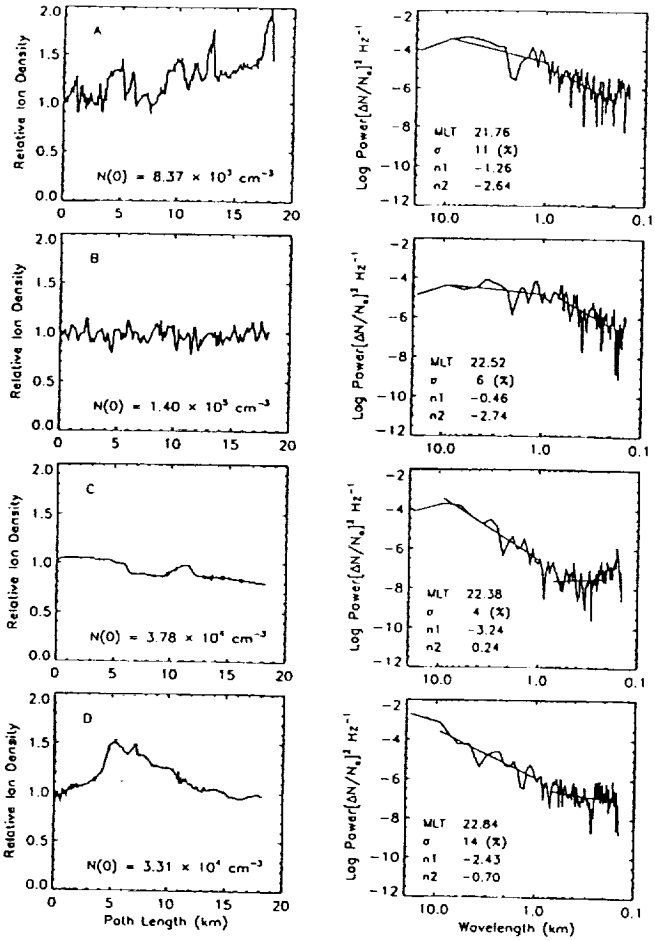

Figure 4. Relative ion density and its power spectrum at the selected four points in Figure 2 (A, B) and Figure 3 (C, D).

Figure 2. The density depletion, irregularity intensity, and power are small compared to those observed at high altitude. The interesting feature is that the spectral index at meter scales (n2) is positive and that at kilometer scales (n1) is small. This kind of spectral form is often observed in the low-altitude region when the irregularity intensity is small. Whether these spectral parameters have physical meaning will be determined after we look into the density structure which produces the given spectrum.

To investigate which density structure produces a given power spectrum, we select two points in each of Figures 2 and 3, and examine the density and its power spectrum in Figure 4. The samples selected in the high-altitude region (A, B) show a large amplitude of density fluctuations and correspondingly the powers for most scale sizes are greater than 10^{-7}. Although the samples A and B are taken at similar altitudes and local times, the irregularity structure at the point A, which is sampled at a bubble center, is significantly different from that at the point B, which is sampled at the edge of a bubble. Inside a bubble (A) the irregularity intensity (σ) is large and the power decreases linearly as the wave number increases. At the outside edge of a bubble or between bubbles (B) the density structure is sinusoidal, which produces a spectral break near 1 km. We will revisit this sinusoidal density structure later.

The samples taken at low altitudes (C, D) show large-scale density modulations without any well-developed irregularity structures. We interpret them as a part of the background structure. At point C the spectrum at kilometer scales is very steep and is more due to the small power at middle scales rather than due to large power at large scales. Small-scale spikes can make powers at the smallest scales relatively large and produce a positive spectral index at meter scales. However, we cannot confidently assign enhanced powers at the smallest scales to a real signal since the spectral density of noise will also produce such signatures. We do not believe that seed perturbations specially favor irregularities of scales less than 200 m. Therefore the spectral index (n2), or more generally, the positive value of it at meter scales, is ignored throughout our analysis. At the point D, middle scale irregularities appear, which makes the spectrum less steep at kilometer scales. The absence or reduced magnitude of irregularities at middle scales in the low-altitude region is the feature of the power spectra that most distinguish them from those in the high-altitude region.

One difficulty met in the study of irregularity evolution is that we know only the present structure but have no direct information about its previous and future state. We just conjecture that observations made at earlier local times may be in the initial or developing phase, while those made at later local times may reflect the properties of the decaying phase. For a few cases the AE-E satellite happened to meet the same irregularity structure at different paths during one night and thus we can investigate the evolution effect directly. Here we will show two cases measured at the low- and high-altitude regions.

The first example is measured on day 77089 at 280 km altitude. During one night the AE-E satellite met the same structure twice with a time separation of about 90 min LT. Figure 5 shows trains of ion density measurements over the two paths. For the convenience of comparison, the density signatures are shifted in time to place the same structure at the same location. The background density is about 10^6 cm^{-3}, so the observation seems to be made near the F peak, although the altitude is low. We are persuaded that PATH 1 is an initial phase and PATH 2 is a developing phase since the density structure at PATH 1 shows very small-amplitude irregularity structures, while that at PATH 2 shows much more developed bubble structures.

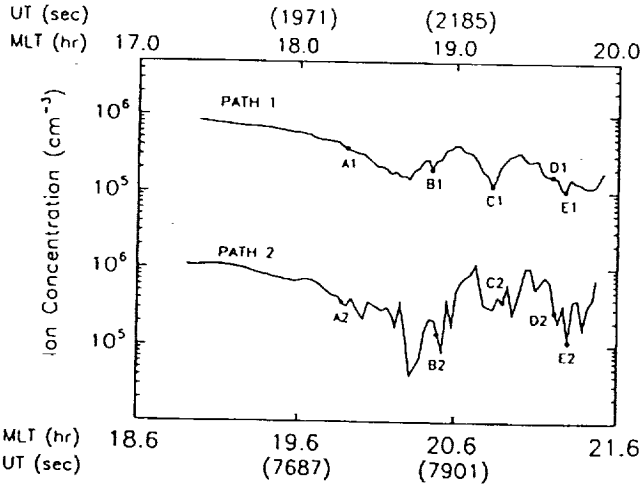

Figure 5. Consecutive measurements of the same structure with an interval of 90 min LT.

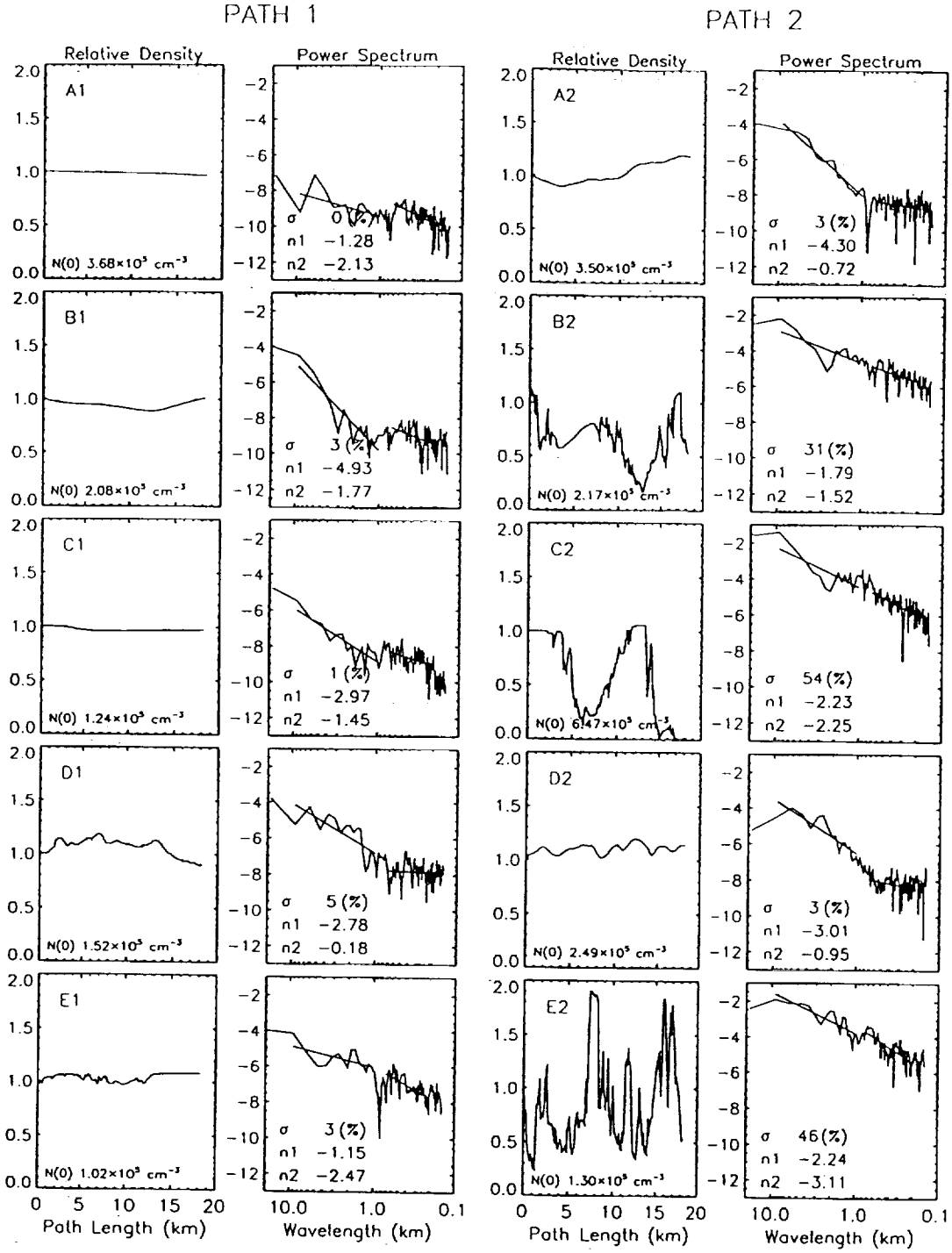

Figure 6. Comparison of density structure and its power spectrum for the two paths shown in Figure 5. Five points are selected from each path which are matched by eye at corresponding locations.

The quiet region (before 1820 LT) and the disturbed region (after 1820 LT) for PATH 1 may be matched to the regions before 2000 LT and after 2000 LT for PATH 2, respectively. It seems that the irregularity structures occupying about 1.5 hours of local time are formed simultaneously and then evolve to another state maintaining the same phase. Therefore the comparison of density structures which are selected from the same path is not appropriate to expose their evolution. The satellite passes through the entire structured region in about 10 min, so we expect the irregularity structures not to change much during that short time. To investigate the density structure and its evolution, we selected five points on each path. Figure 6 shows the relative ion densities and their power spectrum for the selected points. Points A1 and A2, B1 and B2, etc., are matched by eye at corresponding locations. For the samples selected from PATH 1, we cannot see well-developed irregularity structures, and correspondingly the irregularity intensity is less than 5%. At the point A1 there is no

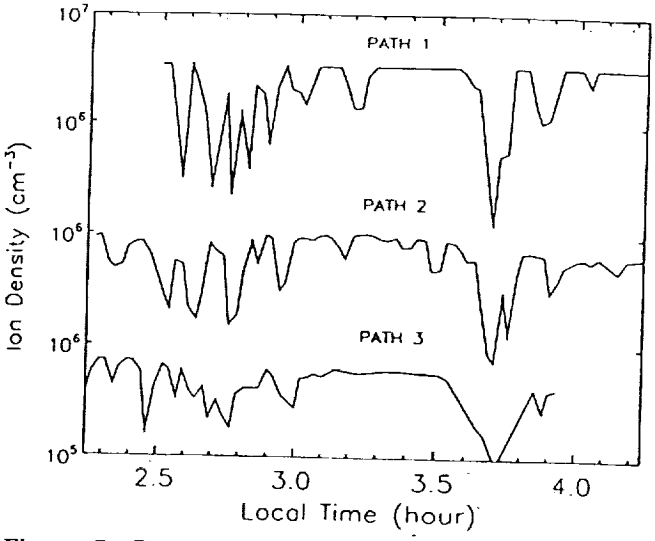

Figure 7. Consecutive measurements of the same structure with an interval of 2 hours LT for each path.

irregularity structure at any scales with power greater than 10^{-7}. The steep slope at kilometer scales for the samples at B1, C1 and D1 is similar to those shown in Figure 4 (C, D). This structure primarily exists in the absence of middle- and small-scale density fluctuations. The presence of small-scale irregularities for the sample E1 increases the power at meter scales, which makes the power spectrum different from the others on PATH 1. Except in case E1, the powers at meter scales are below the noise level and therefore the spectral index (n2) should be ignored.

The bubble-like structures which appear in PATH 2 may be evolving since the bubble depth is still relatively small. The samples B2, C2 and E2 show large density fluctuations for most of the scales, and their power spectrum is essentially linear throughout the range considered without a spectral break near 1 km. It should be noted that the small-scale irregularities are superimposed on larger-amplitude, several-kilometer scale, density modulations. The irregularity intensities (σ) are more than 30%, and they are primarily due to density fluctuations greater than 5 km in scale. It seems that the small-amplitude density modulations for the large scales (λ>5 km) are initially created, and the fluctuation amplitudes increase during the developing phase. In this process the smaller-scale irregularities are created and intensified on the larger-scale gradients.

Another example from which we can investigate the evolution of irregularity structures is found from the measurements on day 79349 at 450 km altitude. Three consecutive passes each spanning a time interval of 2 hours in local time are assumed to be samples of the same structure. Figure 7 shows the trains of ion density for three paths which are adjusted to the local time of PATH 3. The decrease of density depletion level and of the background density for later paths prompt us to conclude that the irregularity structures are in a decaying phase. It seems that the deep and narrow bubbles in PATH 1 become shallower and broader as time progresses.

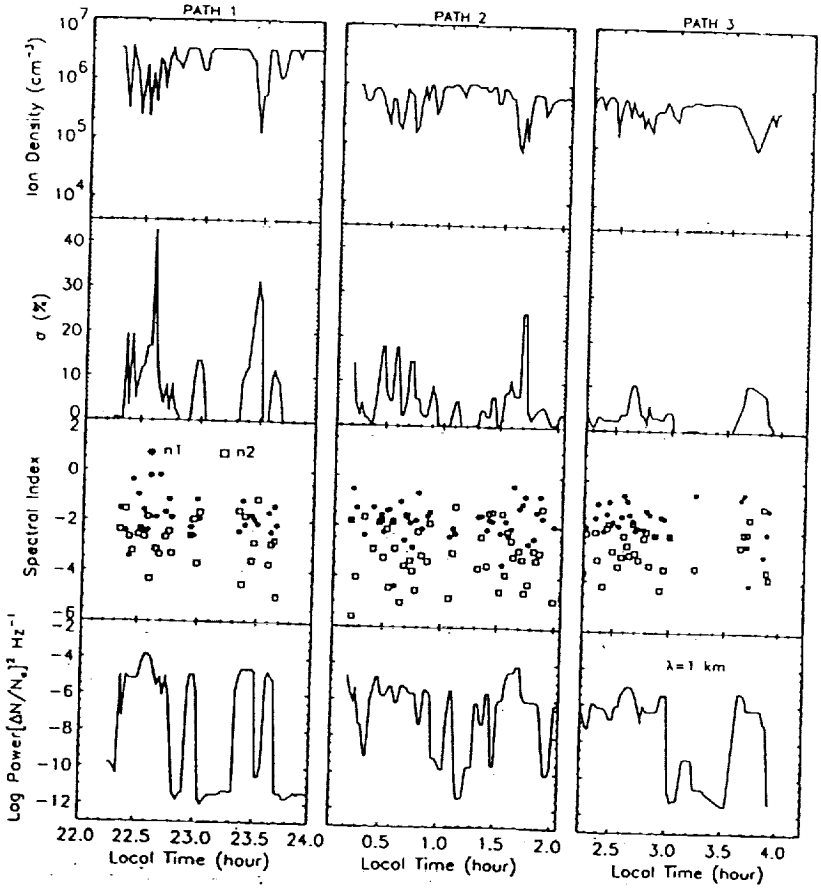

Figure 8. Comparison of spectral parameters for the three paths shown in Figure 7.

We again note that the irregularity structures at each path evolve to another state maintaining the same phase. To compare the spectral characteristics, in Figure 8 we plot ion density, σ, spectral indices, and power at 1 km along each path. As the density depletions decrease from PATH 1 to PATH 3, the irregularity intensity (σ) also decreases a little. However, the changes in spectral indices and power are very small from one path to the other although the local time interval between PATH 1 and PATH 3 is more than 4 hours.

Comparing the evolution pattern on the two days (77089, 79349), we find some different features. The measurements on 77089 show rapid change in irregularity structure in 90 min while those on 79349 show only a small change over intervals of several hours. We note that the first observations (77089) were made at early local times when the irregularity structure is in a developing phase, while the second observations (79349) were made at late local times when the irregularity structure is in a decaying phase. This study demonstrates that the initial perturbations grow rapidly in a short time, but after the irregularities are fully developed, they sustain their state for a long time and decay very slowly.

One interesting aspect we frequently meet in the study of irregularity structure is a spectral break near 1 km. This kind of spectrum is produced by sinusoidal density fluctuations which have primary wavelength near 1 km [*Valladares et al.*, 1983]. We analyze measurements made at 450 km altitude on day 79191 to investigate when and where the spectral break appears. Figure 9 shows the ion density, σ, spectral indices, and power at 1 km in a format the same as Figure 2. The top panel shows three different types of density structures: small amplitude fluctuations, bubble structures, and no irregularity structure. Each case is roughly represented by the regions of σ about 5%, greater than 10%, and zero in the second panel. The third panel shows that the difference in spectral indices between the larger and smaller scales is maximum when σ is about 5%, while it is quite small in the well-structured region. From the fourth panel it is interesting to note that the power at 1 km remains at comparable levels despite the large changes in overall irregularity intensity indicated in the second panel.

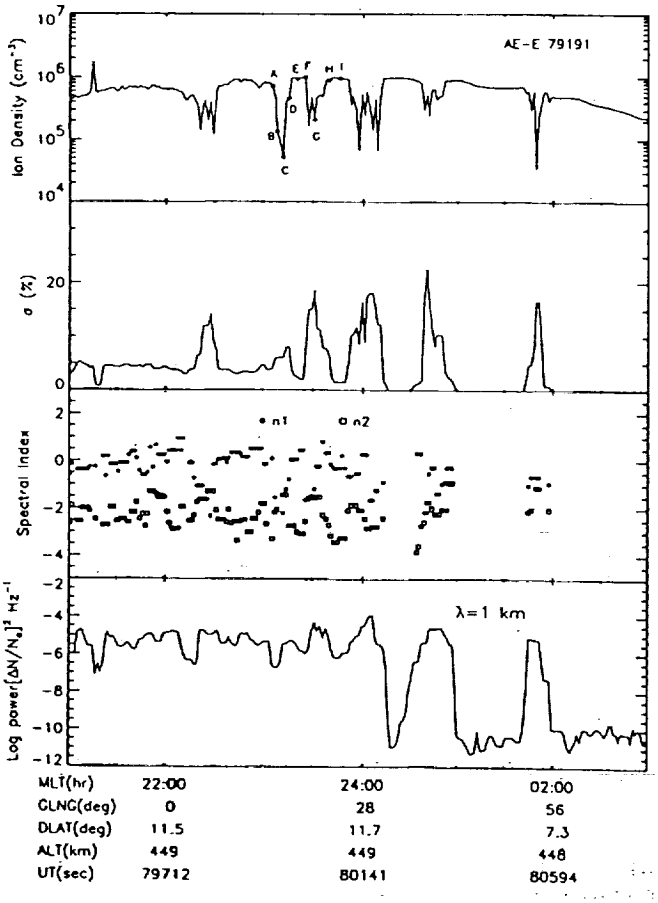

Figure 9. Ion density measurements with σ, spectral index, and power. The difference of spectral indices is large in the region where σ is about 5%.

We select nine points indicated by A-I in the first panel in Figure 9 to study the density structure in detail. Figure 10 shows the relative ion density and power spectrum for the selected points. Samples A, E, H, and I can be classified by the significant presence of sinusoidal density fluctuations which produce a spectral break near 1 km. It is noted that the common locations of this type structure are either outside the boundary of a bubble region or between bubbles. Another distinguishing property is that the background density gradient is almost zero in regions where sinusoidal fluctuations dominate. Even where the density fluctuation is sinusoidal, the fluctuation amplitude is different at different locations. The samples selected at the edge of bubbles (A, H) show larger irregularity intensity than those obtained between bubbles (E, I). The irregularity intensity is usually largest inside bubbles (B, C, D, G), but such locations do not show a dominance of sinusoidal density fluctuations. Sample D shows evidence for a spectral break, although the irregularity structure tends to show increasing amplitude oscillations superimposed on a background. Sample F may also be classified as a sinusoidal density structure if the horizontal density train were truncated prematurely. The main point to be emphasized is that a spectral break generally appears in regions that surround large-scale bubble structures rather than lying within them.

As we have seen from the individual case studies, the density structure and its power spectrum are unexpectedly variable depending on various conditions associated with bubble evolution. To describe the spectral characteristics further, we have produced average spectra for irregularities with intensities greater than 1%. These spectra are examined each 30 min of local time in the range 1700 to 0700 LT.

We first note that the properties of the power spectral density are independent of longitude, and henceforth the discussion will be applied to all longitudes at which ionospheric structure can occur. The rms deviation of the density structure over an extent of 18 km may vary considerably. While we have used a value in excess of 1% to indicate the presence of irregularities, it should be understood that irregularities are typically much larger than this. Since the occurrence region of large irregularity intensity is localized to a few local time hours, any results obtained in that time range will be dominated by the properties of the high-intensity structures. So we have considered separately regions with low-intensity structure ($1\%<\sigma<5\%$) and with high-intensity structure ($\sigma>10\%$). Figure 11 shows the average value of the deviations observed for all irregularities with $1\%<\sigma<5\%$ and $\sigma>10\%$ in the equatorial ionosphere above 350 km and below 300 km altitude. Scatter bars indicate the range of magnitudes observed. For the case $1\%<\sigma<5\%$, the average irregularity intensity increases until 2200 LT and then decays slowly in both of the altitude regions. At high altitudes its magnitude

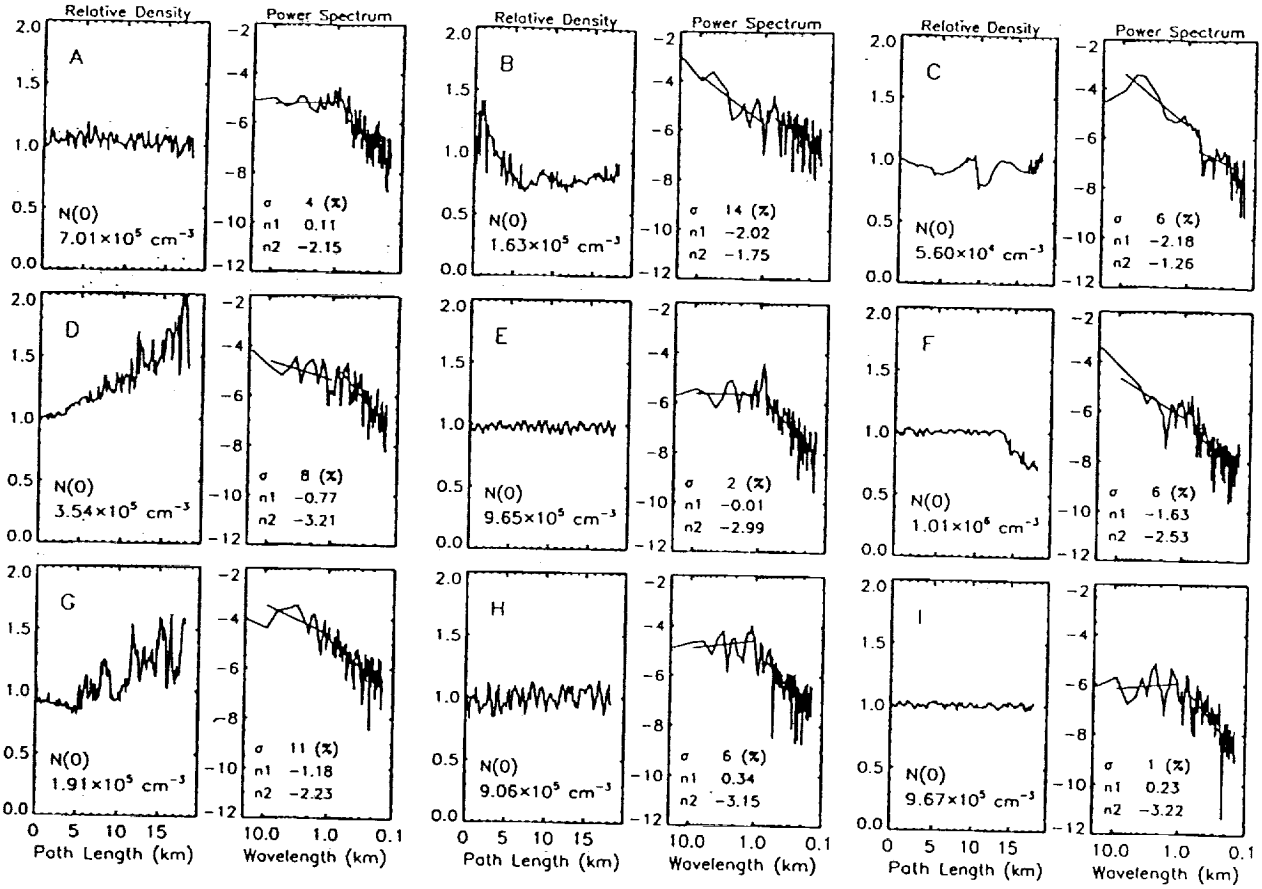

Figure 10. Irregularity structures and their power spectrum at the selected nine points in Figure 9.

persists above 3% until 0300 LT and then drops to 2%. The contribution of sinusoidal density fluctuations will be important during this time when the overall irregularity intensity begins to fall. For $\sigma>10\%$, the irregularity intensity in the high-altitude region increases rapidly after sunset, having its maximum around 2000 LT. Then it decreases rapidly until 2400 LT and slowly after midnight. Most of the intense irregularities are observed before 2400 LT. In the low-altitude region the decay of irregularity intensity occurs very slowly from about 2200 LT onward. The average magnitude of irregularity intensity is the same or larger than that observed at high altitudes, although the density depletions associated with bubbles are generally small in the low-altitude region. The small value of average density (N_o) at low altitudes gives relatively large values of $\Delta N/N_o$.

This description of the evolution of plasma structures with 18-km scale sizes in the nighttime ionosphere does not expose the scale size variations within those structures. This information is contained within the spectral analysis performed here. In this study we limit the minimum observation number to 50 and analyze the data when the average power spectral density at kilometer scales is greater than 10^{-7}. As mentioned previously, the outer-scale limit for these analyses is about 18 km, while the smallest resolved scale size is about 200 m. Figure 12a shows a contour plot of the power spectral density in this scale size range as a function of local time for the low- and high-intensity structures in the altitude region above 350 km. By contrast, Figure 12b shows the same information for ionospheric structures in the altitude region below 300 km. Contour levels in the figures indicate the logarithm of power. Examination of these figures reveals many interesting features of ionospheric structures with the smallest and largest intensities. In the region above 350 km altitude, the behavior is distinctly different from that at lower altitudes. The low-intensity structures are distinguished by a growth in the irregularities with scale sizes less than 10 km. The peak in the magnitude of these structures appears later in local time with increasing scale size. At the largest scales an initial decrease in the power is followed by maintenance at almost fixed levels throughout the night, while the smallest scale sizes decay almost linearly through the night. In this case powers less than about 10^{-4} are assumed to have no physical meaning. By contrast, the high-intensity structures show less distinguishing features dependent on scale size. In this case, following the initial growth of irregularities for about 2 hours after sunset, the smallest- and largest-scale sizes decay to some constant level achieved around 2300 LT. The middle-scale sizes between 3 km and 500 m appear to experience a less rapid decay rate throughout the night.

In the altitude region below 300 km, the variations of power at each scale are quite different from those in the high-altitude region. For the low-intensity structure the powers above 5-km scales maintain constant levels throughout the night, while in the 3-1 km scales, power increases continuously with time. Recall that only powers greater than about 10^{-7} have physical meaning, and therefore we ignore the variations of power at small scales. For the high-intensity structure, the observation number of irregularities is very

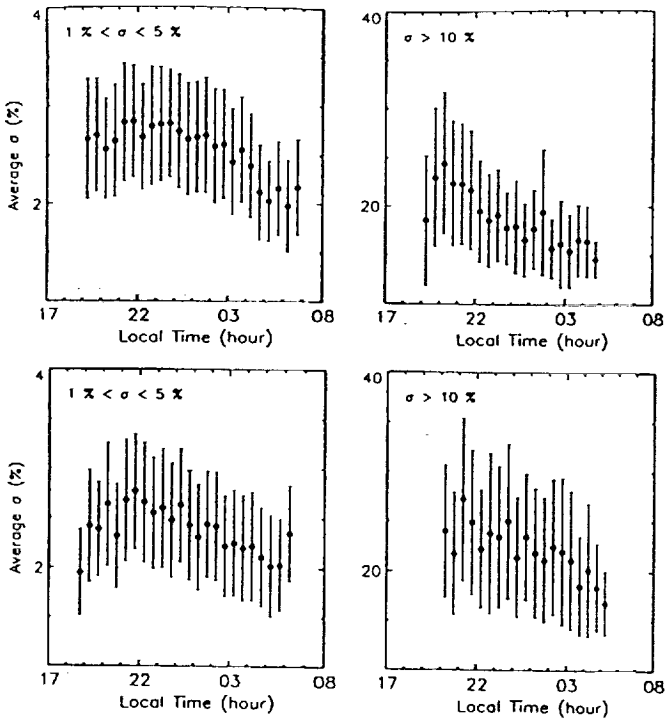

Figure 11. Variations of average irregularity intensity with local time for the low-intensity (1%<σ<5%) and high-intensity (σ>10%) structures in the altitude regions (top) above 350 km and (bottom) below 300 km.

small before 2030 LT. We expect the power for all scales to continuously increase after sunset until 2130 LT. The rapid drop of the power at 2200 LT may be due to the influence of the higher-altitude characteristics.

Figure 13 illustrates the shape of the power spectrum of irregularities that is observed as a result of these evolutionary characteristics at altitudes above 350 km and below 300 km. In this plot each spectrum is normalized to the spectrum at 2330 LT (shown by the thick line) and then shifted by one decade for clarity. Below 300 km altitude we see that, as expected, the spectrum of irregularities for low-intensity structures does not change substantially after 2000 LT. The powers at middle scales increase slowly, which is consistent with the contour map in Figure 12b. For high-intensity structure, the power spectrum maintains almost the same shape through the night. The evolution of the spectrum of irregularities above 350 km altitude is quite striking. The appearance of a "knee" in the spectrum near 1 km appears more distinctly in the lower-intensity structures but is present in all structures. In the low-intensity structures it appears at scale sizes near 500 m and moves to scale sizes near 3 km as local time progresses. Before 2130 LT the increase of power in the middle scale is significant. In the high-intensity structures the "knee" appears near 1 km and shows less obvious movement to other scale sizes as a function of time. It is most important to note that in the low-intensity structures the "knee" is associated with a growth in the irregularity power as a function of time, while in the highest-intensity structures the "knee" forms due to the

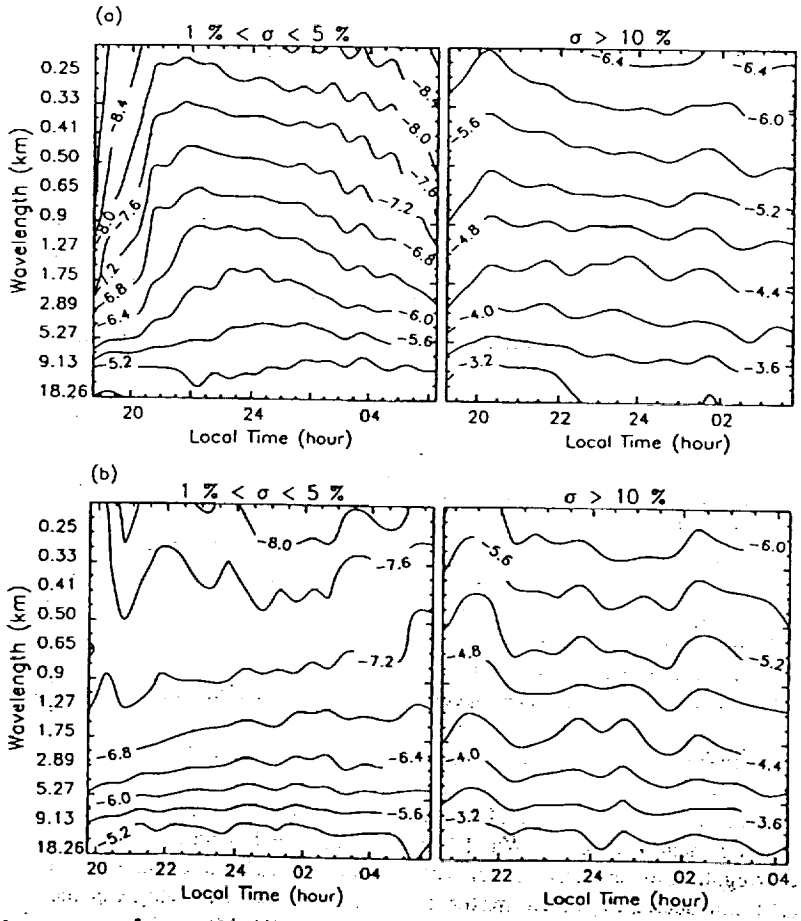

Figure 12. Contour maps of spectral density as a function of local time and spatial scale in the altitude regions (a) above 350 km and (b) below 300 km. Contour levels indicate the logarithm of power.

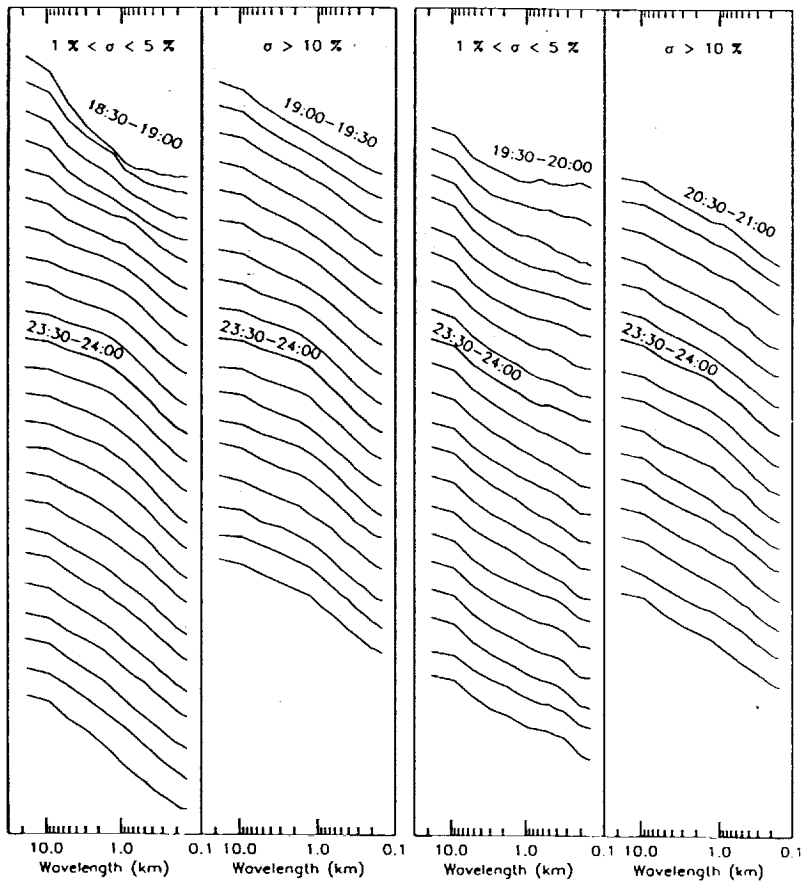

Figure 13. Time evolution of power spectrum for the low- and high-intensity structures in the altitude regions (left) above 350 km and (right) below 300 km.

maintenance of the preferred scale size with respect to the surrounding smaller-and larger-scale sizes. The distinct presence of a break in the power spectrum of irregularities in the scale size regime between 18 km and 200 m means that the spectrum of irregularities is most usefully characterized by two spectral indices. For the purposes of this characterization we make a straight line fit to the log of the power versus the log of the wave number in two-scale size regimes between 10 and 1 km and between 700 and 200 m.

Figure 14a shows the local time evolution of these spectral indices representing the behavior at larger- and smaller-scale sizes at altitudes above 350 km. In this analysis we use a more rigorous restriction for the spectral index at meter scales by excluding those spectra with low powers and positive slopes. In this figure a distinction is also drawn between structures of low and high intensities. The difference of spectral indices and their local time variation are quite significant for low-intensity structure ($1\%<\sigma<5\%$). Until 2200 LT the spectral index at kilometer scales increases rapidly from -2.3 up to -1, while that at meter scales decreases from -2 to -3.2. From the contour map shown in Figure 12a we can see that the large separations in the spectral indices during premidnight hours are due to the increase of power near 1 km until 2400 LT and the decay of small-scale irregularities at early times. After midnight the power near 1 km decreases, which makes the spectrum steep and shallow at kilometer and meter scales, respectively. For the high-intensity structure ($\sigma>10\%$) we can also see an evolution of spectral indices, but we note that the process is different from that for the low-intensity structure. The rapid decay of power at small scales after 2000 LT but the preservation or a little increase of power near 1 km steepens the spectrum at small scales until midnight. Similarly, the shallowing of spectrum at kilometer scales is produced by the decrease of power at the largest scales as well as the preservation of the power near 1 km. After midnight the variation of spectral indices is small, but the slow decrease of power near 1 km makes the spectrum at kilometer scales steepen and the spectrum at meter scales shallow. In the previous individual case study, we observed that, when the structure intensity is large, the fluctuation amplitudes for most scales are also large without any favorite scale. This property does not change much even at late local times and therefore the spectral slope for the high-intensity structure changes little with local time.

The variations of spectral indices are relatively small in the altitude region below 300 km (Figure 14b). For low-intensity structure the spectral index at kilometer scales remains almost constant near -2, while that at meter scales decreases until midnight and then has a constant value near -2.6. This characteristic is closely related to the slow increase of power at middle scales rather than the decrease of power at the largest and the smallest scales. For the high-intensity structure, as we expect from Figure 13, the spectral indices do not change dramatically in time. The absence of any significant

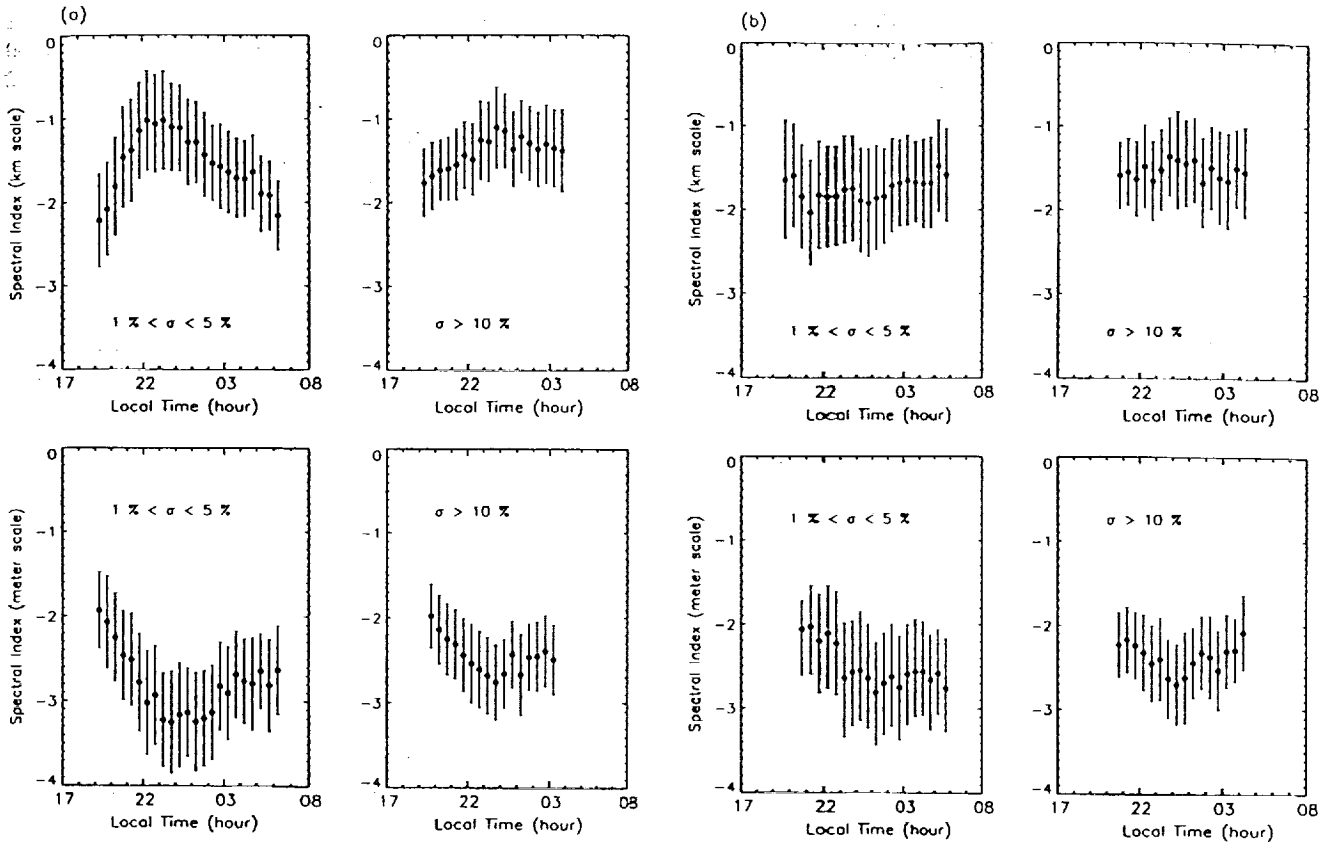

Figure 14. Time evolution of spectral indices in the altitude regions (a) above 350 km and (b) below 300 km.

enhancement or decay of power at middle scales minimizes the variations of spectral indices below 300 km.

4. Discussion

We find a reasonably reproducible local time evolution of the power spectrum of irregularities that is quite different in the altitude regions above 350 km and below 300 km. It should be emphasized that an F peak height that is above the norm is generally associated with the optimum growth of equatorial structures [*Farley et al.*, 1970; *Ossakow and Chaturvedi*, 1978; *Ossakow et al.*, 1979; *Zalesak and Ossakow*, 1980; *Zalesak et al.*, 1982] and thus it is not prudent to associate the observations made above 350 km with the topside and those below 300 km with the bottomside. However, we can assume that those observations below 300 km more closely reflect the properties of the source and those above 350 km more closely reflect the evolutionary characteristics of the ensuing instability processes. It should also be emphasized that the outer scale of the irregularity structures examined here is about 18 km. This is insufficient to expose the presence of very large-scale structures seeded by gravity waves, for example, but is representative of the scales used to assess the impact of irregularities on radio scintillation [*Basu et al.*, 1976].

Several points emerge from examination of this data that are relevant to the effects of irregularities on radio scintillations. First, we note in the scale size regime from 18 to 1 km the spectral index may be significantly different from -2 at any given local time. We find that the spectral index is approximately the same for structure intensities larger than 5% but less intense structures may have significantly different spectral slopes. Above 350 km the irregularity amplitudes grow rapidly between 1800 and 2000 LT. We associate this growth with the action of the Rayleigh-Taylor instability. The growth rate for this instability depends upon the flux tube integrated Pedersen and Hall conductivities [*Anderson and Haerendel*, 1979], and it is important to note that these effective conductivities are dependent on scale size. Additionally, the growth is opposed by cross field diffusion, which is negligible at the large-scale sizes but will inhibit growth at very small scales. We note that the spectral slope of the structures observed above 350 km shallows as a function of local time between 1800 LT and local midnight. This evolution of the spectrum takes place during the initial growth of irregularity amplitude and during its subsequent decay. However, it does show an evolution with local time indicating that structures with scale sizes near 1 km are preserved and may even grow between sunset and 2300 LT.

Two interesting features appear in the study of irregularity structure. Consider first the source irregularity structure on the bottomside. Its properties are best represented by the low-intensity structure rather than by the high-intensity structure. We note that the power at small scales is too low to have any physical meaning. The steep spectrum at kilometer scales is produced by the large-scale density modulations in the absence of irregularities at the middle and smaller scales. The reduced amplitude of middle- and small- scale irregularities is the feature that most distinguishes the spectral characteristics of the low-altitude region from those of the high-altitude region. The density modulations at scales larger than 5 km are assumed

to be a part of the background structure, which is subsequently amplified by the Rayleigh-Taylor instability. On the bottomside, the density depletion level is initially relatively low and therefore the horizontal density gradient is small. In that condition the large-scale irregularities provide little opportunity for the generation of smaller scales since the neutral winds or the drift instability are most effective in regions of steep density gradient. We note also that the Rayleigh-Taylor instability is not effective in the meter-scale regime. The situation is totally different in the high-altitude region. The large background plasma density in the high-altitude region makes the horizontal density gradient very large when the low-density plasma arrives from the bottomside. Then it provides good conditions for the creation of small-scale irregularities by the instability processes. In that case, the middle- and small-scale irregularities are important contributors to the spectral shape.

Another interesting phenomenon is the sinusoidal density structure observed often in the high-altitude region. Basically, the irregularity structure outside a well-structured region or a bubble shows sinusoidal density fluctuations which have primary scale size near 1 km. This structure is observed between 2000 and 0200 LT when the overall structure intensity is low in the high-altitude region. These conditions produce the most significant spectral break in the previous statistical results. The sinusoidal density structure is masked in regions where bubble-like structure appears. It is not always clear whether this structure is created by the rising bubble or already existed before the bubble appears. However, as we can see in Figure 9, the sinusoidal density structures may appear in the regions significantly separated from bubbles, and therefore the latter case may be more realistic. Additionally, observations by *Valladares et al.* [1983] suggest that such structures may exist on the bottomside (and map to the topside) in the absence of bubbles. Note that the high-intensity structures, which show the smallest deviations from a single power law spectrum, occur within depleted regions where the background density N_o is low and thus ΔN may also be low. The lower-intensity structures are more influenced by the presence of irregularities with 1-km scale sizes, that occur in regions where the background density is relatively large. A careful evaluation of the conditions under which irregularities are seen is therefore needed to evaluate their effects on radio scintillation.

The results we obtained from the AE-E satellite measurements agree very well with the study by *Basu et al.* [1978] who have shown the coexistence of kilometer- and meter-scale irregularities, but the meter-scale irregularities decay earlier while the larger scales continue their high spectral intensities for a long time. We have shown that the spectral densities at the smallest scales decay most rapidly before midnight, and the spectral index at meter scales remains very small (steep) after midnight. Thus small scales appear rapidly after sunset and disappear quickly shortly thereafter. This may suggest that small-scale structures are produced, while the larger scales are also developing and thus the instability process may involve the rapid updrafting of depleted plasma. At later local times, when plasma depletions may no longer be convecting rapidly upward, the small-scale structure decays rapidly. For the creation of scintillation in gigahertz, ΔN should be very large [*Basu et al.*, 1976], which corresponds to the large-structure intensity at local times near sunset when background densities are still large. Above 350 km we have shown that the high-structure intensity is observed mostly between 2000 and 2200 LT when the spectral slope in the 10 to 1 km range shallows significantly from -2 to -1.3. The local time corresponds well to the observations of strong gigahertz scintillation, but the impact of higher-intensity irregularities near 1 km as local time increases needs to be examined.

5. Conclusions

We have broadly investigated irregularity structures in the equatorial *F* region and their evolution in time. Low-intensity structure in the altitude region below 300 km is assumed to represent the properties of seed perturbations, and its characteristics are the existence of large spatial scale density modulations (λ>5 km) as a part of the background structure. The absence throughout the night of irregularities at middle scales (3 km>λ>500 m) results in little change in the spectral characteristics with time. This may be contrasted with the large variations of spectral parameters due to the enhancement or decay of spectral densities at middle scales at higher altitudes. Above 350 km, a break in the spectrum near 1 km appears most conspicuously near 2300 LT and exists in structures of all intensities. However, the spectral break is most apparent in low-intensity structures and is primarily caused by the enhancement of irregularity power near 1 km. Irregularity structures change significantly during the developing phase before midnight and then decay retaining their spectral characteristics after midnight. This property is shown consistently from the individual studies and the evolution of average spectral parameters.

The sinusoidal density fluctuations are often observed between 2000 and 0200 LT in the high-altitude region. The standard deviation of these structure is roughly less than 5%. These fluctuations exist at altitudes above 350 km before bubble structures arrive from the bottomside. Further research is required to establish their connection to isolated bottomside perturbations previously observed.

The small scale irregularities are believed to be created after the large-scale irregularities are formed. The neutral winds are expected to act to fragment the large-scale irregularities to small ones and their influence can be identified if we investigate irregularity structure on the east and west walls of a bubble. Therefore the information of neutral winds will be helpful in studying the cascading process from large scale to small scale.

Small-scale irregularities appear to be generated during the early development of large-scale features. The role of neutral winds acting on the horizontal density gradients needs evaluation but so too does the role of vertical velocity shear across such gradients. These mechanisms must account for the early disappearance of small-scale structure despite the continued existence of the large-scale gradients.

Acknowledgments. This work is supported by NASA grant NAGW-4492 and NSF grant ATM-9615064.

The Editor thanks S. L. Ossakow for his assistance in evaluating this paper.

References

Anderson, D. N., and G. Haerendel, The motion of depleted plasma regions in the equatorial ionosphere, *J. Geophys. Res.*, *84*, 4251-4256, 1979.

Basu, S., and S. Basu, Equatorial scintillations: Advances since ISEA-6, *J. Atmos. Terr. Phys.*, *47*, 753-768, 1985.

Basu, S., and C. J. Larson, Turbulence in the upper atmosphere: Effects on satellite systems, *AIAA J. 95-0548*, 1-7, 1995.

Basu, S., S. Basu, and B. K. Khan, Model of equatorial scintillations from in situ measurements, *Radio Sci.*, *11*, 821-832, 1976.

Basu, S., S. Basu, J. Aarons, J. P. McClure, and M. D. Cousins, On the coexistence of kilometer and meter-scale irregularities in the nighttime equatorial *F* region, *J. Geophys. Res.*, *83*, 4219-4226, 1978.

Basu, S., S. Basu, J. P. McClure, W. B. Hanson, H. E. Whitney, High-resolution topside in situ data of electron densities and VHF/GHz scintillations in the equatorial region, *J. Geophys. Res.*, *88*, 403-415, 1983.

Briggs, B. H., and I. A. Parkin, On the variation of radio star and satellite scintillations with zenith angle, *J. Atmos. Terr. Phys.*, *25*, 339-365, 1963.

Chaturvedi, P. K., and S. L. Ossakow, Nonlinear theory of the collisional Rayleigh-Taylor instability in equatorial spread *F*, *Geophys. Res. Lett.*, *4*, 558-560, 1977.

Cragin, B. L., C. E. Valladares, W. B. Hanson, and J. P. McClure, Bottomside sinusoidal irregularities in the equatorial *F* region, 2, Cross-correlation and spectral analysis, *J. Geophys. Res.*, *90*, 1721-1734, 1985.

Dyson, P. L., J. P. McClure, and W. B. Hanson, In situ measurements of the spectral characteristics of *F* region ionospheric irregularities, *J. Geophys. Res.*, *79*, 1497-1502, 1974.

Farley, D. T., B. B. Balsley, R. F. Woodman, and J. P. McClure, Equatorial spread *F*: Implications of VHF radar observations, *J. Geophys. Res.*, *75*, 7199-7216, 1970.

Francis, S. H., and F. W. Perkins, Determination of striation scale sizes for plasma clouds in the ionosphere, *J. Geophys. Res.*, *80*, 3111-3120, 1975.

Hanson, W. B., and R. A. Heelis, Techniques for measuring bulk gas motions from satellites, *Space Sci. Instrum.*, *1*, 493-524, 1975.

Hanson, W. B., R. D. Zuccaro, C. R. Lippincott, and S. Sanatani, The retarding-potential analyzer on atmosphere explorer, *Radio Sci.*, *8*, 333-339, 1973.

Heelis, R. A., and J. F. Vickrey, Magnetic field-aligned coupling effects on ionospheric plasma structure, *J. Geophys. Res.*, *95*, 7995-8008, 1990.

Heelis, R. A., J. F. Vickrey, and N. B. Walker, Electrical coupling effects on the temporal evolution of F layer plasma structure, *J. Geophys. Res.*, *90*, 437-445, 1985.

Kelly, M.C., *The Earth's Ionosphere*, Academic, San Diego, Calif., 1989.

Kelley, M. C., and J. P. McClure, Equatorial spread *F*: A review of recent experimental results, *J. Atmos. Terr. Phys.*, *43*, 427-435, 1981.

Kelley, M. C., R. Pfaff, K. D. Baker, J. C. Ulwick, R. Livingston, and R. Tsunoda, Simultaneous rocket probe and radar measurements of equatorial spread *F*: Transitional and short wavelength results, *J. Geophys. Res.*, *87*, 1575-1588, 1982.

Kelley, M. C., C. E. Seyler, and S. Zargham, Collisional interchange instability, 2, A comparison of the numerical simulations with the in situ experimental data, *J. Geophys. Res.*, *92*, 10,089-10,094, 1987.

Keskinen, M. J., S. L. Ossakow, and P. K. Chaturvedi, Preliminary report of numerical simulations of intermediate wavelength collisional Rayleigh-Taylor instability in equatorial spread *F*, *J. Geophys. Res.*, *85*, 1775-1778, 1980a.

Keskinen, M. J., S. L. Ossakow, and P. K. Chaturvedi, Preliminary report of numerical simulations of intermediate wavelength E × B gradient drift instability in ionospheric plasma clouds, *J. Geophys. Res.*, *85*, 3485-3488, 1980b.

Kil, H., and R.A. Heelis, Global distribution of density irregularities in the equatorial ionosphere, *J. Geophys. Res.*, 103, 407-417, 1998.

LaBelle, J., Mapping of electric field structures from the equatorial F region to the underlying *E* region, *J. Geophys. Res.*, *90*, 4341-4346, 1985.

LaBelle, J., and M. C. Kelley, The generation of kilometer scale irregularities in equatorial spread *F*, *J. Geophys. Res.*, *91*, 5504-5512, 1986.

Livingston, R. C., C. L. Rino, J. P. McClure, and W. B. Hanson, Spectral characteristics of medium-scale equatorial *F* region irregularities, *J. Geophys. Res.*, *86*, 2421-2428, 1981.

Ossakow, S. L., and P. K. Chaturvedi, Morphological studies of rising equatorial spread *F* bubbles, *J. Geophys. Res.*, *83*, 2085-2090, 1978.

Ossakow, S. L., S. T. Zalesak, and B. E. McDonald, Nonlinear equatorial spread *F*: Dependence on altitude of the *F* peak and bottomside background electron density gradient scale length, *J. Geophys. Res.*, *84*, 17-29, 1979.

Rino, C. L., R. T. Tsunoda, J. Petriceks, R. C. Livingston, M. C. Kelley, and K. D. Baker, Simultaneous rocket-borne beacon and in situ measurements of equatorial spread *F*- intermediate wavelength results, *J. Geophys. Res.*, *86*, 2411-2420, 1981.

Rufenach, C. L., Ionospheric scintillation by a random phase screen: Spectral approach, *Radio Sci.*, *10*, 155-165, 1975.

Scannapieco, A. J., and S. L. Ossakow, Nonlinear equatorial spread *F*, *Geophys. Res. Lett.*, *3*, 451-454, 1976.

Singh, M., and E. P. Szuszczewicz, Composite equatorial spread *F* wave number spectra from medium to short wavelengths, *J. Geophys. Res.*, *89*, 2313-2323, 1984.

Sudan, R. N., and M. J. Keskinen, Unified theory of the power spectrum of intermediate wavelength ionospheric electron density fluctuation, *J. Geophys. Res.*, *89*, 9840-9844, 1984.

Valladares, C. E., W. B. Hanson, J. P. McClure, and B. L. Cragin, Bottomside sinusoidal irregularities in the equatorial *F* region, *J. Geophys. Res.*, *88*, 8025-8042, 1983.

Vickrey, J. F., M. C. Kelley, R. Pfaff, and S. R. Goldman, Low-altitude image striations associated with bottomside equatorial spread *F*: Observations and theory, *J. Geophys. Res.*, *89*, 2955-2961, 1984.

Zalesak, S. T., and S. L. Ossakow, Nonlinear equatorial spread *F*: Spatially large bubbles resulting from large horizontal scale initial perturbations, *J. Geophys. Res.*, *85*, 2131-2142, 1980.

Zalesak, S. T., S. L. Ossakow, and P. K. Chaturvedi, Nonlinear equatorial spread *F*: The effect of neutral winds and background Pederson conductivity, *J. Geophys. Res.*, *87*, 151-166, 1982.

Zargham, S., and C. E. Seyler, Collisional interchange instability, 1, Numerical simulations of intermediate-scale irregularities, *J. Geophys. Res.*, *92*, 10,073-10,088, 1987.

R. A. Heelis and H. Kil, William B. Hanson Center for Space Sciences, Physics Program, University of Texas at Dallas, Box 830688, MS FO22, Richardson, TX 75083-0688. (e-mail heelis@utdallas.edu; kil@utd500.utdallas.edu)

(Received August 28, 1997; revised November 14, 1997; accepted November 14, 1997.)